Published in final edited form as:
Biomaterials. 2008 May ; 29(15): 2348–2358.

The Potential to Improve Cell Infiltration in Composite Fiber-Aligned Electrospun Scaffolds by the Selective Removal of Sacrificial Fibers

Brendon M. Baker[1,2], **Albert O. Gee, MD**[1], **Robert B. Metter**[1,2], **Ashwin S. Nathan**[1,2], **Ross L. Marklein**[2], **Jason A. Burdick, PhD**[2], and **Robert L. Mauck, PhD**[1,2*]

1*McKay Orthopaedic Research Laboratory, Department of Orthopaedic Surgery, University of Pennsylvania, Philadelphia, PA 19104*

2*Department of Bioengineering, University of Pennsylvania, Philadelphia, PA 19104*

Abstract

Aligned electrospun scaffolds are a promising tool for engineering fibrous musculoskeletal tissues as they reproduce the mechanical anisotropy of these tissues and can direct ordered neo-tissue formation. However, these scaffolds suffer from a slow cellular infiltration rate, likely due in part to their dense fiber packing. We hypothesized that cell ingress could be expedited in scaffolds by increasing porosity, while at the same time preserving overall scaffold anisotropy. To test this hypothesis, poly(ε-caprolactone) (a slow-degrading polyester) and poly(ethylene oxide) (a water-soluble polymer) were co-electrospun from two separate spinnerets to form dual-polymer composite fiber-aligned scaffolds. Adjusting fabrication parameters produced aligned scaffolds with a full range of sacrificial (PEO) fiber contents. Tensile properties of scaffolds were a function of the ratio of PCL to PEO in the composite scaffolds, and were altered in a predictable fashion with removal of the PEO component. When seeded with mesenchymal stem cells (MSCs), increases in the starting sacrificial fraction (and porosity) improved cell infiltration and distribution after three weeks in culture. In pure PCL scaffolds, cells lined the scaffold periphery, while scaffolds containing >50% sacrificial PEO content had cells present throughout the scaffold. These findings indicate that cell infiltration can be expedited in dense fibrous assemblies with the removal of sacrificial fibers. This strategy may enhance *in vitro* and *in vivo* formation and maturation of a functional constructs for fibrous tissue engineering.

Keywords

Tissue Engineering; Mechanical Properties; Cellular Infiltration; Nanofiber; Fibrous Scaffolds; Electrospinning; Anisotropy; Mesenchymal Stem Cells

Introduction

Connective tissues such as tendons, ligaments, and the knee menisci serve critical load-bearing roles and their fibrous architectures are organized to optimize mechanical function [1–3]. This

*Corresponding Author: Robert L. Mauck, PhD, Assistant Professor of Orthopaedic Surgery and Bioengineering, McKay Orthopaedic Research Laboratory, Department of Orthopaedic Surgery, University of Pennsylvania, 424G Stemmler Hall, 36th Street and Hamilton Walk, Philadelphia, PA 19104, Phone: (215) 898-3294, Fax: (215) 573-2133, Email: lemauck@mail.med.upenn.edu.

organization imbues these tissues with anisotropic properties that are highest in the fiber direction. The demanding environment in which these tissues perform predisposes them to damage and endogenous repair processes do not restore tissue structure or function. Instead, highly-ordered tissue is replaced by a disorganized and mechanically inferior scar that is prone to re-injury [4,5]. Thus, there exists an unmet need for an implantable tissue substitute for fiber-reinforced tissues.

Towards this end, investigations have focused on electrospun scaffolds composed of aligned nano- and micro-scale fibers [6–10]. These fibrous scaffolds are formed by electrospinning, wherein polymeric jets are drawn through a voltage gradient and collected layer-by layer on a grounded surface [11]. Numerous polymers have been electrospun, including non-degradable and degradable synthetics as well as biopolymers (for review, see [12]). These fibers mimic the length scales of native cellular microenvironments and enhance matrix deposition [13]. When collected on rotating mandrels, near complete fiber alignment can be achieved, resulting in controllable mechanical and structural anisotropy [7,10,14,15]. Aligned scaffolds mimic fiber-reinforced tissue organization, and can serve as a 3D micropattern for neotissue formation. Using poly(ε-caprolactone) (PCL) fibrous scaffolds, we showed that mesenchymal stem cells (MSCs) aligned, deposited collagen, and increased construct tensile properties in the fiber direction [10,16]. Conversely, when seeded on randomly-oriented scaffolds, disorganized orientations and matrix deposition was observed, with smaller mechanical improvements.

While aligned scaffolds show promise for fiber-reinforced tissues, several limitations remain. Most significantly, cell infiltration into these dense structures is slow. In aligned scaffolds in particular, fiber packing increases density and reduces pore size, limiting cellular ingress. In slow-degrading aligned PCL meshes, human and bovine meniscus fibrochondrocytes infiltrated only the outer two-thirds of 1mm thick scaffolds after ten weeks [16,17]. Although it is not known if complete infiltration would have occurred with longer culture durations, more rapid colonization is clearly required for clinical applications.

To address this issue, a number of methodologies for improving infiltration have been proposed. Most directly, cells have been electrosprayed into forming scaffolds [18]. However issues of layering, sterility, and time (to produce thicker scaffolds) may limit this application. Others have noted that synthetic polymers are not amenable to biologic remodeling, and so have electrospun biopolymers including collagen, elastin, and fibrinogen [12,19,20]. One study compared cell infiltration into electrospun collagen or polyester meshes implanted in rat muscle, and reported that synthetic scaffolds were minimally colonized while collagen scaffolds were fully infiltrated after one week [21]. However, the mechanical properties of electrospun biopolymers are much lower than most synthetic meshes, even after crosslinking [22,23], limiting their application to non-load bearing situations.

Another method for improving infiltration may be by increasing porosity. Work with porous foams and sponges suggests that there exists an optimal pore size for cell infiltration [24]. For fibrous scaffolds, this approach has been addressed by mixing different diameter fibers [25]. Alternatively, pores have been introduced by including salt particles at the time of production (which are subsequently leached out) [26]. This technique improves cell infiltration, though at the expense of macroscopic delaminations.

As our goal is to create and preserve structural anisotropy to foster fiber-reinforced tissue formation, we developed an approach based on the inclusion of sacrificial fibers in a composite fibrous scaffold. We hypothesized that the selective removal of sacrificial fibers would increase porosity and accelerate cell infiltration. We also hypothesized that the mechanical properties of composite scaffolds before and after sacrificial fiber removal would reflect the fractions of

each population, and that anisotropy would be preserved. To test these hypotheses, we developed a dual-electrospinning process to create aligned scaffolds containing a slow degrading and a sacrificial component. PCL and poly(ethylene oxide) (PEO) were utilized based on their degradation and dissolution times; PCL degrades slowly and serves as a structural element, while PEO dissolves in aqueous solution and serves as the sacrificial component. Using this system, we created fully interspersed fibrous constructs containing a range of sacrificial fractions. We evaluated the mechanical properties of these scaffolds in their 'as formed' state and after removal of the sacrificial component. Further, we measured MSC infiltration after 3 weeks into composite scaffolds with a range (0–90%) of sacrificial fractions.

Materials and Methods

Formation of Single-Polymer and Composite Fibrous Scaffolds

In this study, composite fiber-aligned fibrous scaffolds were produced by dual-component electrospinning. A 14.3% w/v solution of PCL (80kDa, Sigma-Aldrich, St. Louis, MO) was made in a 1:1 mixture of tetrahydrofuran and N,N-dimethylformamide (Fisher Chemical, Fairlawn, NJ) by stirring at 40°C for 18 hours. PEO (200kDa, Polysciences, Inc., Warrington, PA) was dissolved in 90% ethanol with stirring at room temperature for six hours to yield a 10% w/v solution. The polymer solutions were electrospun using a custom electrospinning device to generate fiber-aligned meshes comprised of PCL, PEO, or a mixture of discrete PCL and PEO fibers (Figure 1). To electrospin each component, separate 20ml syringes were filled with PCL or PEO and fitted with a 5cm length of flexible silicon tubing connected to a 12" long stainless steel 18G blunt-ended needle that served as the charged spinneret. Spinnerets reciprocated over an 8cm path (6.4cm/sec) along the mandrel under the control of two custom-built 'fanners'. The flow rate of both solutions was maintained at 2.5ml/h via syringe pump (KDS100, KD Scientific, Holliston, MA). A power supply (ES30N-5W, Gamma High Voltage Research, Inc., Ormond Beach, FL) was used to apply a +13kV potential difference between the spinnerets and the grounded aluminum mandrel (Ø=2"), which was rotated via a belt mechanism conjoined to an AC motor (Pacesetter 34R, Bodine Electric, Chicago, IL) to achieve a linear velocity of ~10m/s. PCL and PEO fibers were collected over a spinneret-mandrel distance of 15 and 10cm, respectively. Additionally, two aluminum shields charged to +10kV were placed perpendicular to and on either side of the mandrel to better direct the electrospun fibers towards the grounded mandrel.

Three distinct types of fiber meshes were formed. Pure PCL and PEO meshes were generated by electrospinning the respective single polymer from one spinneret. A 60:40 PCL/PEO dual-polymer scaffold was produced by aligning the axes of the two opposing spinnerets (Figure 1; offset distance, D=0). From each of these three fiber mats, 30mm long by 5mm wide strips were excised in either the fiber or transverse-fiber direction (with the long-axis of strip parallel or perpendicular to the predominant fiber direction, respectively). Samples of each scaffold type and fiber orientation were divided into two groups (n=3/group), one of which was immediately tensile tested as-spun (AS) while the other was tested post-submersion (PS), after removal of the PEO fibers. PS samples were weighed dry, submerged with agitation in 90% EtOH for three hours followed by distilled water for an additional three hours. PS samples were then dehydrated overnight in a vacuum desiccator and reweighed to determine mass loss. Percentage mass loss was taken as an indication of the PEO content of dual-polymer samples, as pure PCL scaffolds did not change with this treatment.

In order to tune different compositions in dual-polymer composite scaffolds, the above setup was modified by offsetting the axes of the spinnerets (i.e., offset distance, D=4cm). This setup produced a graded fiber mesh ranging from nearly pure PCL at one end of the mandrel to nearly pure PEO at the other end. 25mm long by 5mm wide strips were excised in the fiber direction for analysis of mass loss and mechanical properties under AS and PS conditions as described

above. From the same graded fiber mesh, samples indexed to mandrel position were excised for investigation of cellular infiltration. This fibrous mesh was generated over the course of six hours, resulting in a fiber mat ranging in thickness from 0.56 to 0.92 mm (0.80 ± 0.10mm).

Visualization of Sacrificial Fiber Removal

To confirm the presence and interspersion of the two different fiber populations, PCL and PEO solutions were doped with Cell Tracker Red at 0.001% w/v or fluorescein at 0.01% w/v, respectively, and co-electrospun onto glass slides affixed to the rotating mandrel. Fibers were collected for one minute and imaged before and after PEO fiber removal at 20× using a Nikon T30 inverted fluorescent microscope equipped with a CCD camera and the NIS Elements software (Nikon Instruments, Inc., Melville, NY). Additionally, both AS and PS full thickness scaffolds (pure PCL and 60:40 PCL/PEO) were examined by scanning electron microscopy. Samples were AuPd sputter coated and imaged with a JEOL 6400 scanning electron microscope (Penn Regional Nanotechnology Facility) operating at an accelerating voltage of 11kV.

Mechanical Testing of Single-Polymer and Composite Scaffolds

Uniaxial tensile testing was carried out on AS and PS samples cut in the fiber and transverse to the fiber directions using an Instron 5848 Microtester equipped with serrated vise grips and a 50N load cell (Instron, Canton, MA). Prior to mechanical testing, three thickness measurements along the length of each sample were taken and averaged with a custom LVDT measurement system; three width measurements were acquired and averaged in similar fashion using a digital caliper. Samples were preloaded for 60 seconds to ensure proper seating and engagement of the sample; scaffolds cut in the fiber direction were loaded to 0.5N while those cut in the transverse-fiber direction were loaded to 0.25N. After noting the gauge length with a digital caliper, the sample was preconditioned with extension to 0.5% of the gauge length at a frequency of 0.1Hz for 10 cycles. Subsequently, the sample was extended to failure at a rate of 0.1% of the gauge length per second. Stiffness was determined over a 3% strain range from the linear region of the force-elongation curve using a custom MATLAB script. Incorporating sample geometry and the noted gauge length, a tensile modulus was calculated from the analogous portion of the stress-strain curve. Maximum stress was determined from the maximum load achieved by the sample normalized to its starting cross-sectional area.

Cell Seeding and Assessment of Cell Infiltration

MSCs were isolated from the tibial trabecular bone marrow of two 3–6 month old calves (Research 87, Inc., Boylston, MA) as in [16]. The proximal end of the tibia was sectioned and marrow freed from the trabecular spaces via shaking in DMEM supplemented with 300units/ml heparin. After centrifugation for 5 minutes at 500*g*, the pelleted matter was resuspended in DMEM containing 1X Penicillin/Streptomycin/Fungizone (PSF) and 10% Fetal Bovine Serum (FBS) and plated in 150mm tissue culture dishes. Adherent cells formed numerous colonies through the first week, and were subsequently expanded through passage 2 at a ratio of 1:3.

Six squares (5×5mm) cut from the graded PCL/PEO fiber mat describe above were sterilized and rehydrated with decreasing concentrations of ethanol (100, 70, 50, 30%; 30 minutes/step). A 20μl aliquot containing 100,000 MSCs was loaded onto each side of the scaffold followed by one hour of incubation to allow for cell attachment. Cell-seeded scaffolds were cultured in non-tissue culture treated 6-well plates with 3mL of chemically-defined medium (high glucose DMEM with 1X PSF, 0.1μM dexamethasone, 50μg/mL ascorbate 2-phosphate, 40μg/mL L-proline, 100μg/mL sodium pyruvate, 1X ITS+ (6.25μg/ml Insulin, 6.25μg/ml Transferrin, 6.25ng/ml Selenous Acid, 1.25mg/ml Bovine Serum Albumin, and 5.35μg/ml Linoleic Acid) with 10ng/mL TGF-β3), changed twice weekly.

After three weeks of culture, samples were removed from culture and gross morphology was recorded via stereomicroscope. Samples were then fixed in 4% phosphate-buffered paraformaldehyde and embedded in Optimal Cutting Temperature compound (OCT, Sakura Finetek USA, Inc., Torrance, CA). 8μm thick cross-sections were cut with a Cryostat (Microm HM500, MICROM International GmbH, Waldorf, Germany) and stained with Prolong Gold Antifade with DAPI (Invitrogen) to visualize cell nuclei. Fluorescent and phase images of each sample were obtained at 4× as above.

Cell infiltration was quantified with a custom MATLAB script (The Mathworks, Inc., Natick, MA). This program was written to minimize user bias and to speed data processing. The phase image of the construct cross-section was displayed and the user manually defined the periphery of the scaffold. At ten evenly-spaced positions along the periphery, the minimal distance to the adjacent face was determined; these ten measurements were averaged to yield the scaffold thickness. The user-defined boundary was then mapped to the corresponding DAPI image which had been threshholded and clustered. The threshholding level was selected to maximize noise removal without hampering the detection of nuclei; as all images were obtained at the same brightness and exposure time, this level was maintained for all image processing. The clustering algorithm scanned the threshholded image searching for groups of contiguous white pixels, resulting in the demarcation of each cell nucleus by a cluster of pixels. The minimal distance between the user-defined scaffold periphery and the centroid of each cluster was calculated. To account for variation in scaffold thickness, each nucleus-to-boundary distance was normalized to the scaffold thickness to produce a percentage infiltration relative to the scaffold center. For each PCL/PEO formulation, six independently cultured samples were sectioned, imaged, and processed as above.

Composite Scaffold Model

To better appreciate the dynamic characteristics of the composite scaffolds, a custom MATLAB script was written to model scaffolds with varying PEO content. A 1000 by 1000 pixel area was populated by 3 pixel diameter fibers whose angles ranged between ± 20° from the vertical axis. This angular deviation was taken from [10] who measured angular dispersion of aligned fibers created using similar parameters. Fiber starting position was randomly assigned along the top edge and fibers were extended towards the bottom edge according to the randomly assigned angle. To model a layer of a X:100-X PCL/PEO scaffold, a total of 2·X fibers were produced. Thus, a 100% PCL scaffold contains 200 fibers and a 50:50 PCL/PEO scaffolds contains only 100 fibers, as PEO fibers are removed upon scaffold wetting. The void spaces defined by the fibrous array were then quantified and measured using a clustering algorithm (function bwlabeln, MATLAB Image Processing Toolbox). Total pore size, pore number, and the distribution of pore sizes were outputted for each of 20 model iterations, with a new random fiber starting position and angle generated with each iteration.

Statistical Analysis

Analysis of variance and Pearson's correlations were carried out with SYSTAT (v10.2, Point Richmond, CA) with Fisher's LSD post-hoc tests used to make pair-wise comparisons between groups. A level of significance was set at $p \leq 0.05$. For the assessment of single- and dual-polymer scaffold mechanical properties, five samples/group were analyzed. From the graded PCL/PEO fiber mesh, three samples/group were analyzed for mechanical properties and six samples/group were evaluated in cellular studies. Data are presented as the mean ± the standard deviation.

Results

Production and Evaluation of Composite Fibrous Scaffolds

Composite scaffolds containing both individual PCL and PEO fibers were produced using the electrospinning device shown in Figure 1. For these initial studies, the spinnerets were positioned in direct opposition, resulting in a fiber mesh containing ~60% PCL and ~40% PEO (as determined by mass loss after wetting, 41.6 ± 0.3%). Fluorescent-labeling of the fibers within the scaffold (PCL: red, PEO: green) demonstrated that fibers could be successfully interspersed by co-electrospinning (Figure 2A). Submersion of the scaffold in an aqueous environment showed rapid removal of PEO fibers, leaving PCL fibers intact (Figure 2B). SEM visualization of these 60:40 PCL/PEO scaffolds as formed showed dense fibers organized along a predominant direction. After submersion in the aqueous solution, scaffolds appeared less dense and larger inter-fibrillar voids or pore spaces were apparent. At some junctions, small deposits were visible, likely indicative of a small PEO component remaining after this short period of aqueous incubation. Despite the removal of a significant fraction of the fiber population, the overall fiber alignment was retained (Figure 2C, 2D).

Tensile Properties of Single- and Dual-Polymer Composite Scaffolds

To determine the effect of fiber interspersion on the mechanical properties of the composite scaffolds, tensile testing was performed on as-spun (AS) pure PCL, pure PEO, and 60:40 PCL/PEO scaffolds. Testing was carried out both in the fiber direction and perpendicular or transverse to the fiber direction. After evaluating the as-spun (AS) properties, paired samples for the PCL and PEO/PCL groups were tested post-submersion (PS) to examine the effect of fiber removal on tensile behavior. Pure PEO samples dissolved completely with submersion and could not be mechanically tested. Example stress-strain plots of samples tested in the fiber direction are shown in Figure 3A. From these plots, it is evident that pure PCL and PEO scaffolds possess a different mechanical response; PCL scaffolds show a significant toe region and a large post-yield linear extension while PEO scaffolds lacked a toe region and failed soon after reaching its yield point. Composite scaffolds containing a mixture of both polymers showed characteristics of each individual constituent. AS PCL/PEO samples lacked a toe region (similar to pure PEO) but showed a long post-yield extension region (similar to pure PCL). After submersion in aqueous solution, the stress-strain profile of PS PCL/PEO samples was similar to pure PCL, though overall these scaffolds reached lower stress levels, indicative of the lower PCL fiber fraction present.

Quantification of these results showed that, in the fiber direction, AS PCL/PEO scaffolds reached similar maximum stresses as pure PCL ($p=0.354$) and that both groups were significantly higher than the pure PEO scaffolds ($p<0.001$). As expected, exposure of pure PCL scaffolds to aqueous solution did not change their tensile performance ($p=0.783$). Conversely, the same treatment of PCL/PEO scaffolds resulted in a decline in the maximum stress achieved compared to AS PCL/PEO and PS PCL samples ($p<0.001$). PCL samples tested in the transverse direction were distensible beyond the range of the testing device, and thus comparisons of maximum stress could not be made in this direction.

Tensile moduli were calculated from the linear portion of the stress-strain curves of scaffolds tested in the fiber or transverse directions. Pure PEO scaffolds had a higher modulus (36.5 ± 7.5MPa) than pure PCL scaffolds (16.1 ± 1.5MPa) when tested in the fiber direction ($p<0.001$, Figure 3C). Similar findings were observed in the transverse direction (PEO: 6.6 ± 0.3MPa; PCL: 1.4 ± 0.1MPa, $p<0.001$). The modulus of composite 60:40 PCL/PEO scaffolds in the fiber direction (20.6 ± 1.0MPa) trended higher than pure PCL ($p=0.054$), reflecting the contributions of the stiffer PEO component. In the transverse direction this difference in tensile modulus was significant ($p<0.001$ vs. pure PCL). Submersion in an aqueous environment had

no effect on PCL in either direction ($p>0.55$), but resulted in a decrease in modulus in the composite PCL/PEO scaffolds in both testing directions ($p<0.005$). The anisotropy ratio (AR) was calculated by normalizing the fiber direction modulus to that of the transverse-fiber direction. With submersion, the AR of PCL was unaffected (AS: 11.51±0.63 vs. PS: 11.67 ±0.08) but that of PCL/PEO more than doubled (AS: 7.17±0.38 vs. PS: 16.43±0.18), due in part to the larger relative decline in properties in the transverse direction.

Tuning Scaffold Composition and Mechanics

To explore the relationship between sacrificial fiber content and tensile properties of the composite scaffolds, the PCL and PEO fiber jets were offset from one another and a graded PCL/PEO fiber sheet was generated. This sheet transitioned along the length of the mandrel from a nominal PEO content at one terminus to >90% PEO content at the other, as determined by the amount of mass lost with submersion (Figure 4A). Increasing the fraction of PEO fibers included in the as-spun (AS) scaffolds led to a larger decline in tensile properties when these fibers were removed. The maximum load and stiffness of samples post submersion (PS) were normalized that of their respective AS scaffolds (Figure 4B, 4C). Both maximum load and stiffness showed a significant negative correlation with the % PEO removed ($R^2=0.87$, $p<0.001$ and $R^2=0.99$, $p<0.001$, respectively). These findings indicate that scaffold mechanics may be tuned according to the PEO content initially present.

MSC Infiltration into Fibrous Scaffolds with Increasing Sacrificial Content

To determine whether sacrificial fiber removal would affect cell infiltration, scaffolds removed from graded PCL/PEO meshes were seeded with MSCs and cultured for three weeks. Gross scaffold morphology and nuclear position within the scaffold were evaluated for a number of starting PEO contents (Figure 5). DAPI staining of construct cross-sections was used to assess the depth of infiltration into and distribution of cells throughout the scaffolds. Overall, cellular infiltration improved with increasing starting PEO content. For example, with 5% PEO, cells were present only at the periphery, with no cells reaching the middle third of the scaffold. At 50% PEO, cells reached the central region, though some regions remained devoid of cells. At 60% PEO, nearly complete infiltration was observed. Still further improvements in cell infiltration were seen at higher PEO contents. However, at these higher PEO contents, significant distortions of the starting scaffold shape was observed.

To quantify these findings, cellular infiltration was evaluated from phase and DAPI images taken of construct cross-sections (Figure 6A, 6B). The boundary of the fibrous scaffold (FS) was defined from the phase image and only cells within these boundaries were analyzed. This excluded the contributions from the cell sheath (CS) that forms on all scaffolds. Next, the shortest distance between each cell nucleus and the FS periphery was measured and normalized to the sample's half-thickness, yielding a percent infiltration. Thus when cells reach the center of the scaffold, 100% infiltration is achieved (Figure 6B). Results of this analysis showed that the % infiltration increased with PEO contents >40% (Figure 6C). Samples beyond 60% PEO could not be analyzed in this fashion due to their misshapen boundaries. To further this analysis, we also determined cellular distribution within the scaffold with varying PEO content. The % infiltration of each cell was determined and binned into ranges of 0–25% (outermost), 25–50%, 50–75%, and 75–100% (central region). These counts were normalized to the total number of cells within each scaffold. Results of this analysis for the lowest and highest PEO contents (5 and 60% PEO) are shown in Figure 6D, and the full range is quantified in Figure 6E. In the 0–25% infiltration range, the 5% PEO scaffolds contained a significantly higher fraction of cells than the 60% PEO group ($p<0.001$). Conversely, in the 25–50% range, 60% PEO scaffolds contained more cells than 5% PEO ($p<0.001$). This shift towards increased infiltration became more exaggerated in the 50–75% bin ($p<0.001$). Finally, ~10% of the total cell population reached the center-most region for 60% PEO scaffolds, while no cells were present in this same

region for the 5% PEO group. When considering all groups between 5 and 60% PEO content, a loose, but significant negative correlation was observed between percentage of cells in the outermost 0–25% region with increasing PEO content ($p<0.05$). Conversely, the opposite trend was found in the 50–75% range, with an increasing percentage of the total cell population occupying this region with higher starting PEO contents ($p<0.005$).

Modeling Pore Size in Composite Scaffolds with Increasing Sacrificial Content

To better understand the effect of scaffold porosity on cellular infiltration, a simple mathematical model was created. Composite scaffolds occupying a single layer were generated with a range of starting PEO contents (0–95%) Representative scaffolds with 10, 50, and 90% of the total fibers removed are shown, depicting composite PCL/PEO scaffolds after submersion to remove the PEO content (Figure 7A). Analysis of the number of pores in these virtual scaffolds showed a steady decrease in pore number with increasing % PEO removal (Figure 7B). As the number of pores diminished, the average pore size increased. This change in average pore size steadily increased until 60% PEO, after which an exponential growth was observed. To evaluate pore size distribution in these composite scaffolds, the size of each pore in 10, 50, and 90% PEO content scaffolds was calculated, binned logarithmically, and reported as a percentage of the total pore number. Both 10% and 50% PEO layers behaved similarly, with the majority of pores below 10,000 pixels. However, a notable shift was observed in 90% PEO layers, where the bulk of pores were between 10,000 and 100,000 pixels in size.

Discussion

Aligned micro- and nano-fibrous scaffolds are a promising vehicle for the engineering of fiber-reinforced tissues of the musculoskeletal system. In past work, we have shown that such scaffolds can promote ordered ECM deposition and functional maturation in the fiber direction. However, considerable culture times were required to achieve full cellular colonization of even relatively thin scaffolds (~1mm). To address this issue, we developed a dual-polymer electrospinning process that intersperses a sacrificial fiber component within a composite fibrous scaffold. We hypothesized that the selective removal of these sacrificial fibers would increase scaffold porosity, and thereby accelerate cell infiltration.

To test this hypothesis, we developed a co-electrospinning process to produce and collect fibers from two distinct spinnerets. This blending process has previously been employed by several investigators to produce interspersed fibers within a randomly oriented fibrous assembly [27–29]. In the present study (Figure 2) we show that interspersion of discrete fibers of differing composition can be achieved, while maintaining the organized fiber directionality within the scaffold. Furthermore, we show that combining individual fiber components with dissimilar mechanical properties influences the composite scaffold mechanics, and does so as a function of the fiber fractions employed. The modulus of PCL/PEO composite scaffolds was higher than pure PCL as a result of the inclusion of the stronger PEO component (Figure 3). Notably, this inclusion also altered several key features of the stress-strain profile, including the toe region and the plastic deformation response of the scaffolds after reaching their yield point.

In this dual-component electrospinning process, water-soluble PEO was chosen as the sacrificial fiber component. Both visual inspection and mechanical testing of scaffolds before and after removal of PEO fibers indicated that mechanical anisotropy was preserved. Further, we were able to show that by offsetting the source spinnerets with respect to one another, a graded fibrous mesh could be produced with varying PEO contents. The tensile properties (both in terms of maximum stress, stiffness, and modulus) reflected the amount of sacrificial component removed from the scaffold. Indeed, a linear relationship was found between PEO content removed and overall scaffold properties (Figure 4). These findings are consistent with the work of Ding and coworkers, who showed that differences in the mechanical properties in

blended non-aligned meshes could be achieved by varying the relative number of spinnerets focused on a centralized collecting surface [27]. Collectively, these results suggest that a tunable range of material properties can be achieved in these composite fibrous scaffolds.

To assess the degree to which removal of this sacrificial fiber population influenced cellular ingress, graded sacrificial content scaffolds were produced and seeded with MSCs for three weeks. MSCs were chosen for this application as they can assume a number of different phenotypes [30,31], and have been used in various attempts to engineer fibrous tissues with fibrous scaffolds [16,32]. At the end of the culture period, cellular infiltration was assessed by quantifying the position of nuclei within the scaffold cross-section. A demonstrable improvement in cellular infiltration was observed with removal of the sacrificial fiber fraction (Figure 5), particularly in meshes that started with greater than 40% sacrificial component. In scaffolds with 5% PEO content, more than 80% of the cells resided in the outer 25% of the scaffold. Conversely, increasing the sacrificial PEO component to 60% resulted in less than 50% of the total cell population in this edge region. Instead, cells were found to migrate to a greater degree into the central regions of the scaffold. Indeed, in the 60% PEO scaffold, >10% of the total cells had reached the center at three weeks, while no cells had done so in the 5% PEO group. Evaluating scaffolds with a range of starting PEO contents showed that these trends were consistent across the groups considered. These findings show that cell infiltration into dense aligned fibrous scaffolds can be improved with removal of a sacrificial component.

One finding of interest in this study was that the improvement in cell infiltration only occurred above a certain threshold value of starting sacrificial content (in this case, at about 40%). To better understand this phenomenon, we created a simple model of composite scaffolds, and analyzed pore number, average pore size, and individual pore distribution within a series of ‘virtual’ scaffolds representing those produced experimentally. Results of this model show, as expected, a decrease in the number of pores and an increase in average pore size with increasing fiber removal. Unexpectedly, a marked transition from steady growth in average pore size to rapid changes in this parameter with further fiber removal was observed between 70% and 90% sacrificial fiber content. While this is a planar model and is not necessarily correlative with the experimental results of this study (in that a threshold exists over which cells invade to a greater extent), this finding is illustrative of the non-linear responses possible with sacrificial removal from these composite scaffolds.

While the results of this study are promising, several key limitations remain to be addressed. Although cell infiltration was improved, an even distribution throughout the scaffold was not achieved. Under the best conditions analyzed (~60% sacrificial fiber removal), ~45% of cells remain in the outer ¼ of the scaffold, and only ~12% progressed into the central ¼. Additionally, this study was only designed to assess cellular position, and did not explore the cell-mediated production of extracellular matrix or changes in mechanical properties of these scaffolds with time culture. In previous studies we have shown that collagen deposition is localized to areas of high cell density, and that a strong positive correlation exists between scaffold tensile properties and collagen content [16,17]. Future studies will determine if longer culture durations result in a more even distribution of cells and matrix, and whether this process produces more rapid maturation and/or higher mechanical properties in these scaffolds.

Another limitation found in this study was the dimensional stability of the cell-seeded scaffolds at higher sacrificial fiber contents. We observed a threshold of sacrificial fiber removal above which cell infiltration increased markedly. However, in this same domain, significant changes in construct dimensions were observed. Most likely, this was due to cell-mediated contraction as unseeded PS scaffolds did not demonstrate comparable behavior. This suggests that the remaining fiber component was not sufficiently robust to resist this distortion. Control over this dimensional change could be affected in a number of ways. Scaffold peripheries might be

clamped to maintain the as-formed shape of the construct. This is analogous to approaches that use rigid fixation of the boundaries of cell seeded-collagen gels, which contract significantly if left un-tethered [33]. Alternatively, the slow-degrading polymer could be altered to achieve greater structural resilience to deformation. For example, Li and coworkers have shown that fibrous PGA scaffolds are markedly stiffer in tension than PCL scaffolds [23]. Based on the linear relationship we observed in this study between sacrificial content and stiffness, a composite PGA/PEO scaffold would be expected to have higher tensile properties at any level of PEO content, and may therefore better resist contraction than the composite PCL-based scaffolds employed here. However, PGA is less elastically deformable than PCL which might limit application of the composite in certain physiologic scenarios. Alternatively, an entirely different class of polymers could be utilized. We have recently electrospun elements of a novel photopolymerizable library of poly(β-amino ester)s [34,35]. These polymers have a wide range of tensile properties (modulus and elongation prior to yield), and so could be selected to specifically meet the design requirements. Another possibility is to use several polymers in a multi-polymer blend, rather than simply the two different components used in this study. In this work we created a situation in which increased porosity is either present or absent immediately after submersion in an aqueous environment. Tailoring overall degradation with the inclusion of a third component which degrades on a medium (weeks to months) time scale may maintain scaffold dimensions while still promoting cellular infiltration over the entire time course.

Conclusions

In conclusion, this study demonstrated that inclusion and subsequent removal of a sacrificial fiber population within a fiber-aligned fibrous scaffold enhances cellular infiltration. Moreover, removal of these sacrificial elements preserved structural and mechanical anisotropy, and could be tuned to generate composites with varying mechanical properties. The finding of increased rates of cell infiltration may similarly increase the rate of biochemical and mechanical maturation of these constructs, improving their efficacy at producing a functional tissue replacement, either *in vitro* or after *in vivo* implantation. While further work is required to optimize this process, these results suggest that sacrificial fibers provide one route for overcoming a significant barrier to the use of these dense, fibrous structures.

Acknowledgements

This work was funded in part by a pilot grant from the Penn Center for Musculoskeletal Disorders (RLM, NIH AR050950), a University of Pennsylvania University Research Foundation Award (RLM and JAB), and a Graduate Research Fellowship from the National Science Foundation (BMB).

References

1. Lynch HA, Johannessen W, Wu JP, Jawa A, Elliott DM. Effect of fiber orientation and strain rate on the nonlinear uniaxial tensile material properties of tendon. J Biomech Eng 2003;125(5):726–731. [PubMed: 14618932]
2. Setton LA, Guilak F, Hsu EW, Vail TP. Biomechanical factors in tissue engineered meniscal repair. Clin Orthop Relat Res 1999;(367 Suppl):S254–S272. [PubMed: 10546651]
3. Holzapfel GA, Schulze-Bauer CA, Feigl G, Regitnig P. Single lamellar mechanics of the human lumbar anulus fibrosus. Biomech Model Mechanobiol 2005;3(3):125–140. [PubMed: 15778871]
4. Newman AP, Anderson DR, Daniels AU, Dales MC. Mechanics of the healed meniscus in a canine model. Am J Sports Med 1989;17(2):164–175. [PubMed: 2667375]
5. Beredjiklian PK, Favata M, Cartmell JS, Flanagan CL, Crombleholme TM, Soslowsky LJ. Regenerative versus reparative healing in tendon: a study of biomechanical and histological properties in fetal sheep. Ann Biomed Eng 2003;31(10):1143–1152. [PubMed: 14649488]

6. Reneker DH, Chun I. Nanometre diameter fibres of polymer, produced by electrospinning. Nanotech 1996;7:216–223.
7. Courtney T, Sacks MS, Stankus J, Guan J, Wagner WR. Design and analysis of tissue engineering scaffolds that mimic soft tissue mechanical anisotropy. Biomaterials 2006;27(19):3631–3638. [PubMed: 16545867]
8. Ayres C, Bowlin GL, Henderson SC, Taylor L, Shultz J, Alexander J, et al. Modulation of anisotropy in electrospun tissue-engineering scaffolds: Analysis of fiber alignment by the fast Fourier transform. Biomaterials 2006;27(32):5524–5534. [PubMed: 16859744]
9. Li WJ, Mauck RL, Tuan RS. Electrospun nanofibrous scaffolds: production, characterization, and applications for tissue engineering and drug delivery. J Biomed Nanotech 2005;1(3):259–275.
10. Li WJ, Mauck RL, Cooper JA, Yuan X, Tuan RS. Engineering controllable anisotropy in electrospun biodegradable nanofibrous scaffolds for musculoskeletal tissue engineering. J Biomech 2007;40(8): 1686–1693. [PubMed: 17056048]
11. Deitzel JM, Kleinmeyer J, Harris D, Beck Tan NC. The effect of processing variables on the morphology of electrospun nanofibers and textiles. Polymer 2001;42:261–272.
12. Li M, Mondrinos MJ, Gandhi MR, Ko FK, Weiss AS, Lelkes PI. Electrospun protein fibers as matrices for tissue engineering. Biomaterials 2005;26(30):5999–6008. [PubMed: 15894371]
13. Li WJ, Jiang YJ, Tuan RS. Chondrocyte phenotype in engineered fibrous matrix is regulated by fiber size. Tissue Eng 2006;12(7):1775–1785. [PubMed: 16889508]
14. Nerurkar NL, Elliott DM, Mauck RL. Mechanics of oriented electrospun nanofibrous scaffolds for annulus fibrosus tissue engineering. J Orthop Res 2007;25(8):1018–1028. [PubMed: 17457824]
15. Ayres CE, Bowlin GL, Pizinger R, Taylor LT, Keen CA, Simpson DG. Incremental changes in anisotropy induce incremental changes in the material properties of electrospun scaffolds. Acta Biomater 2007;3(5):651–661. [PubMed: 17513181]
16. Baker BM, Mauck RL. The effect of nanofiber alignment on the maturation of engineered meniscus constructs. Biomaterials 2007;28(11):1967–1977. [PubMed: 17250888]
17. Baker BM, Nathan AS, Huffman GR, Mauck RL. Tissue Engineering of Meniscus Constructs with Autologous Human Fibrochondrocytes Derived from Surgical Debris. Osteoarthritis and Cartilage. 2007
18. Stankus JJ, Guan J, Fujimoto K, Wagner WR. Microintegrating smooth muscle cells into a biodegradable, elastomeric fiber matrix. Biomaterials 2006;27(5):735–744. [PubMed: 16095685]
19. Buttafoco L, Kolkman NG, Engbers-Buijtenhuijs P, Poot AA, Dijkstra PJ, Vermes I, et al. Electrospinning of collagen and elastin for tissue engineering applications. Biomaterials 2006;27(5): 724–734. [PubMed: 16111744]
20. McManus MC, Boland ED, Koo HP, Barnes CP, Pawlowski KJ, Wnek GE, et al. Mechanical properties of electrospun fibrinogen structures. Acta Biomater 2006;2(1):19–28. [PubMed: 16701855]
21. Telemeco TA, Ayres C, Bowlin GL, Wnek GE, Boland ED, Cohen N, et al. Regulation of cellular infiltration into tissue engineering scaffolds composed of submicron diameter fibrils produced by electrospinning. Acta Biomater 2005;1(4):377–385. [PubMed: 16701819]
22. Matthews JA, Wnek GE, Simpson DG, Bowlin GL. Electrospinning of collagen nanofibers. Biomacromolecules 2002;3(2):232–238. [PubMed: 11888306]
23. Li WJ, Cooper JA Jr. Mauck RL, Tuan RS. Fabrication and characterization of six electrospun poly (alpha-hydroxy ester)-based fibrous scaffolds for tissue engineering applications. Acta Biomater 2006;2(4):377–385. [PubMed: 16765878]
24. van Tienen TG, Heijkants RG, Buma P, de Groot JH, Pennings AJ, Veth RP. Tissue ingrowth and degradation of two biodegradable porous polymers with different porosities and pore sizes. Biomaterials 2002;23(8):1731–1738. [PubMed: 11950043]
25. Pham QP, Sharma U, Mikos AG. Electrospun Poly(epsilon-caprolactone) Microfiber and Multilayer Nanofiber/Microfiber Scaffolds: Characterization of Scaffolds and Measurement of Cellular Infiltration. Biomacromolecules 2006;7(10):2796–2805. [PubMed: 17025355]
26. Nam J, Huang Y, Agarwal S, Lannutti J. Improved cellular infiltration in electrospun fiber via engineered porosity. Tissue Eng 2007;13(9):2249–2257. [PubMed: 17536926]

27. Ding B, Kimura E, Sato T, Fujita S, Shiratori S. Fabrication of blend biodegradable nanofibrous nonwoven mats via multi-jet electrospinning. Polymer 2004;45(6):1895–1902.

28. Kidoaki S, Kwon IK, Matsuda T. Mesoscopic spatial designs of nano- and microfiber meshes for tissue-engineering matrix and scaffold based on newly devised multilayering and mixing electrospinning techniques. Biomaterials 2005;26(1):37–46. [PubMed: 15193879]

29. Madhugiri S, Dalton A, Gutierrez J, Ferraris JP, Balkus KJ Jr. Electrospun MEH-PPV/SBA-15 composite nanofibers using a dual syringe method. J Am Chem Soc 2003;125(47):14531–14538. [PubMed: 14624602]

30. Johnstone B, Hering TM, Caplan AI, Goldberg VM, Yoo JU. In vitro chondrogenesis of bone marrow-derived mesenchymal progenitor cells. Exp Cell Res 1998;238:265–272. [PubMed: 9457080]

31. Caplan AI. Mesenchymal stem cells. J Orthop Res 1991;9(5):641–650. [PubMed: 1870029]

32. Li WJ, Tuli R, Huang X, Laquerriere P, Tuan RS. Multilineage differentiation of human mesenchymal stem cells in a three-dimensional nanofibrous scaffold. Biomaterials 2005;26(25):5158–5166. [PubMed: 15792543]

33. Costa KD, Lee EJ, Holmes JW. Creating alignment and anisotropy in engineered heart tissue: role of boundary conditions in a model three-dimensional culture system. Tissue Eng 2003;9(4):567–577. [PubMed: 13678436]

34. Anderson DG, Tweedie CA, Hossain N, Navarro SM, Brey DM, Van Vliet KJ, et al. A Combinatorial Library of Photocrosslinkable and Degradable Materials. Advanced Materials. 2007In press

35. Tan AR, Ifkovits JL, Baker BM, Brey DM, Mauck RL, Burdick JA. Electrospinning of Photocrosslinked and Degradable Fibrous Scaffolds. J Biomed Mater Res. 2008in press

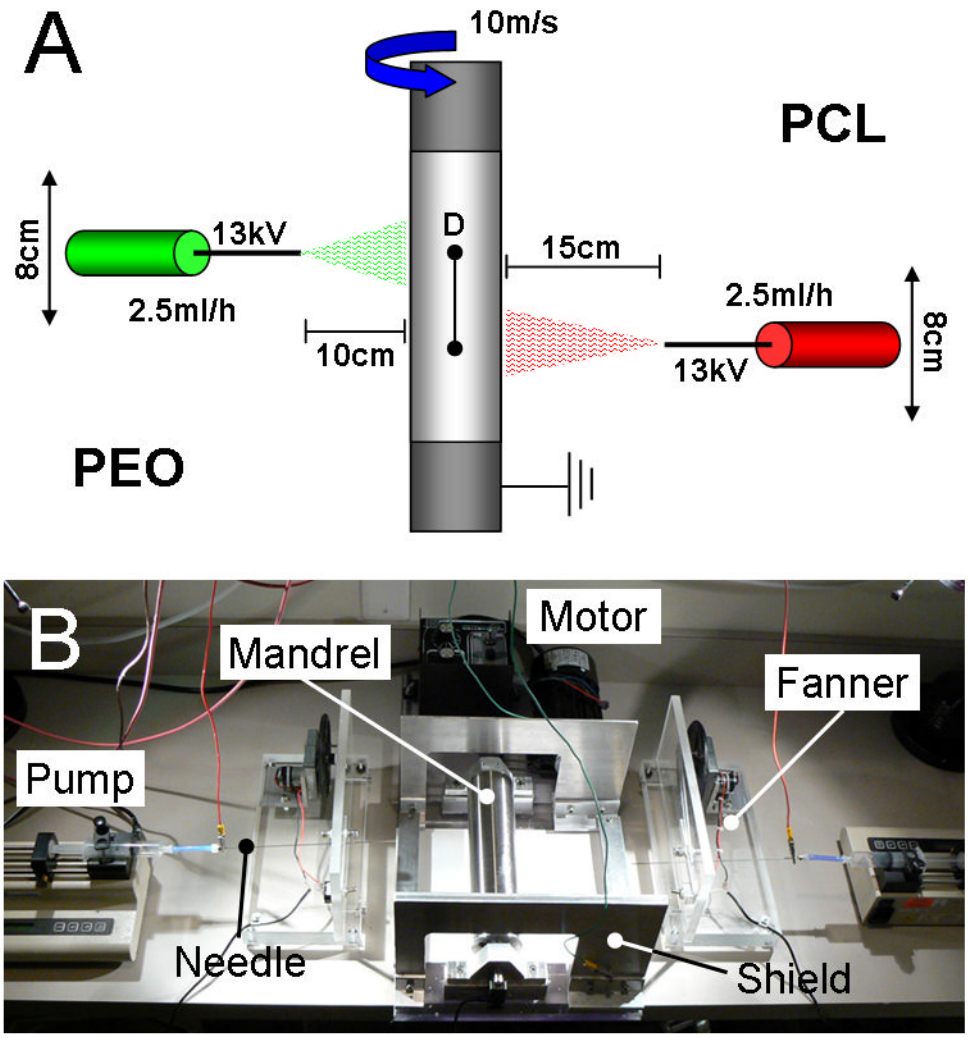

Figure 1. Electrospinning setup for the fabrication of dual-polymer composite fibrous scaffolds

(A) Schematic depicting the electrospinning parameters implemented in generating PCL (red), PEO (green), and PCL/PEO composite scaffolds. (B) The electrospinning apparatus in operation with two syringe pumps delivering polymers distributed by 'fanners' along a common rotating mandrel.

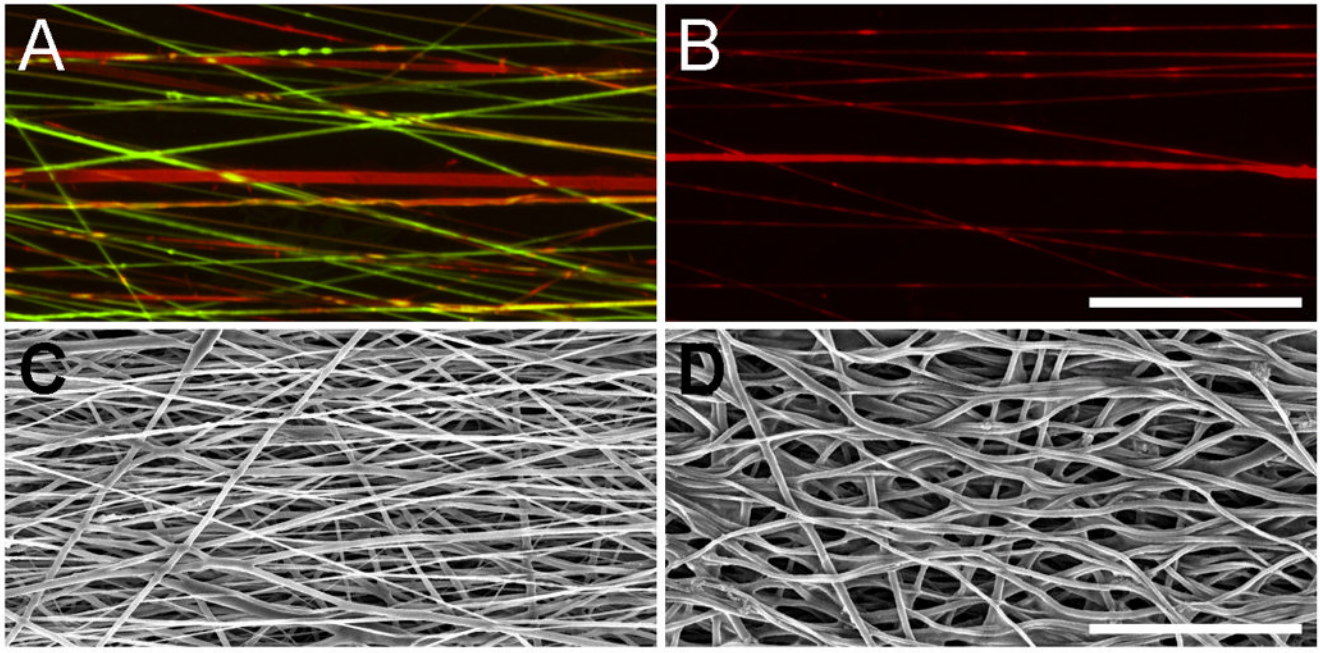

Figure 2. Composite fibrous scaffolds can be formed with individual fibers of distinct polymer composition. Removal of one sacrifical fiber population increases scaffold porosity

(A) Fluorescently-labeled PCL (red) and PEO (green) fibers showed pronounced alignment and interspersion. (B) Submersion of scaffolds in an aqueous solution removed the PEO component while the PCL fibers remained intact. SEM images of as-spun (C) and post-submersion (D) composite scaffolds reveal increases in pore size with the removal of sacrificial PEO fibers. Scale bars: 50 μm.

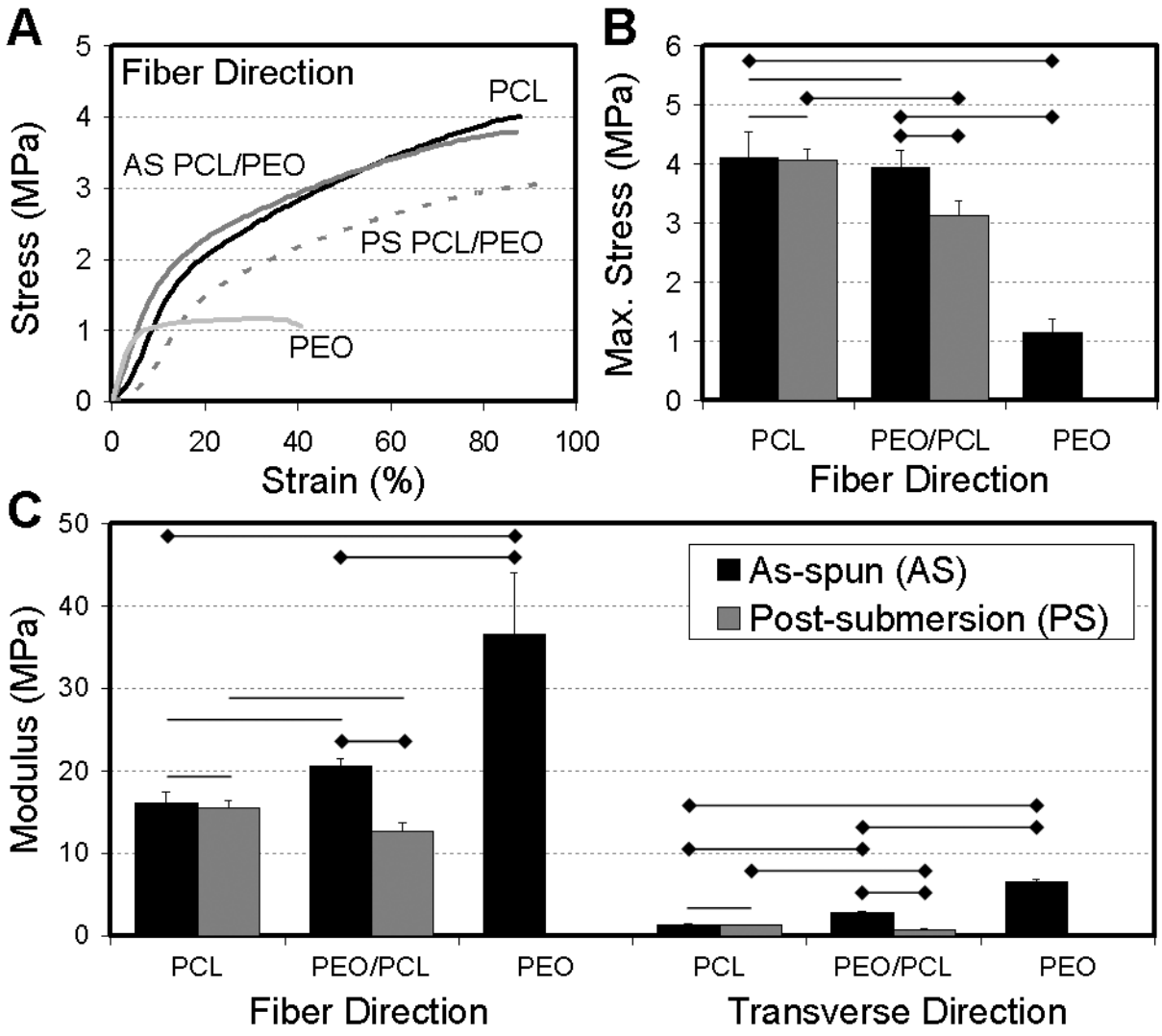

Figure 3. The tensile properties of composite scaffolds is modulated by both the interspersion of multiple polymer components in distinct fibers, as well as by the removal of sacrificial fiber components

(A) Example stress-strain behavior of pure PCL, pure PEO, and PCL/PEO scaffolds as-spun (AS) and post-submersion (PS). (B) Maximum tensile stress achieved by samples from each group when tested in the fiber direction. (C) Tensile modulus of AS and PS samples from each group tested in the fiber and transverse directions. Note that pure PEO scaffolds dissolved completely upon submersion, and so could not be mechanically evaluated. Diamond-ended lines (◆) indicate significance with $p<0.05$; unmarked lines denote no significant difference between groups; n=5/group.

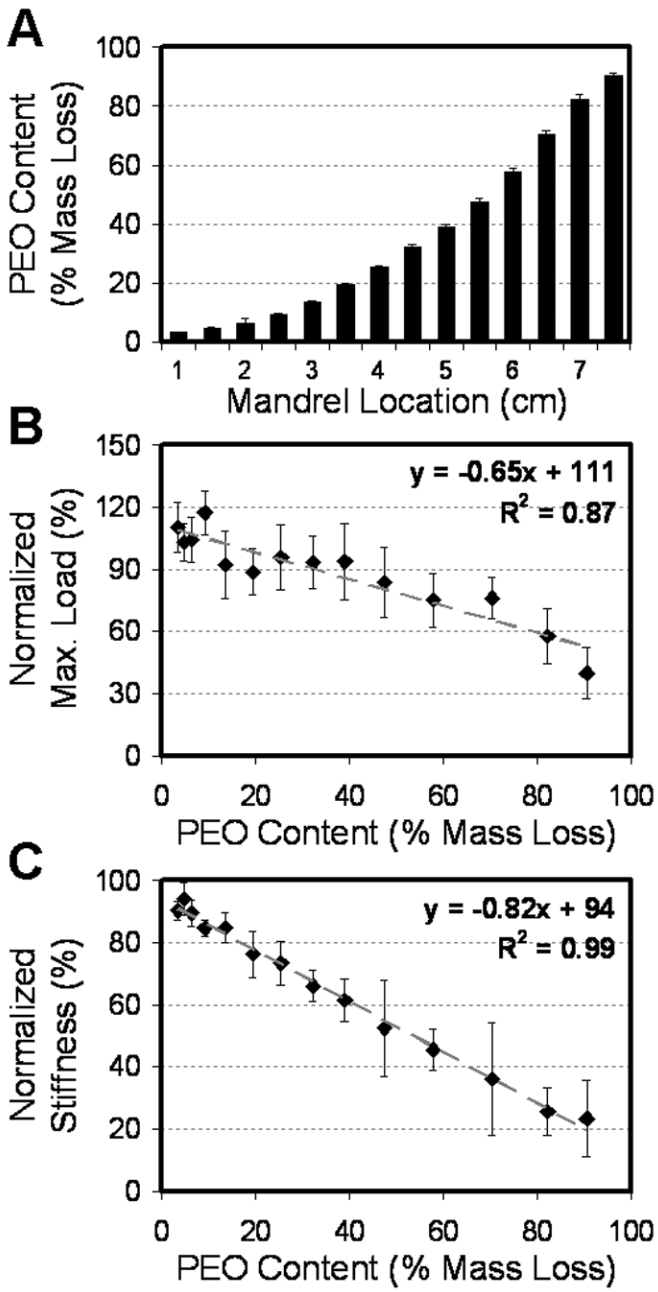

Figure 4. The composition and tensile properties of composite scaffolds can be tuned along the length of the mandrel

(A) Off-setting spinnerets results in a graded fiber sheet ranging from nominal (~5%) to ~90% PEO content along the mandrel as determined by PS mass loss. Scaffold % PEO content correlated with maximum stress (B) and modulus (C) when samples were tested in the fiber direction. Correlations were significant with $p<0.001$; n=3/group.

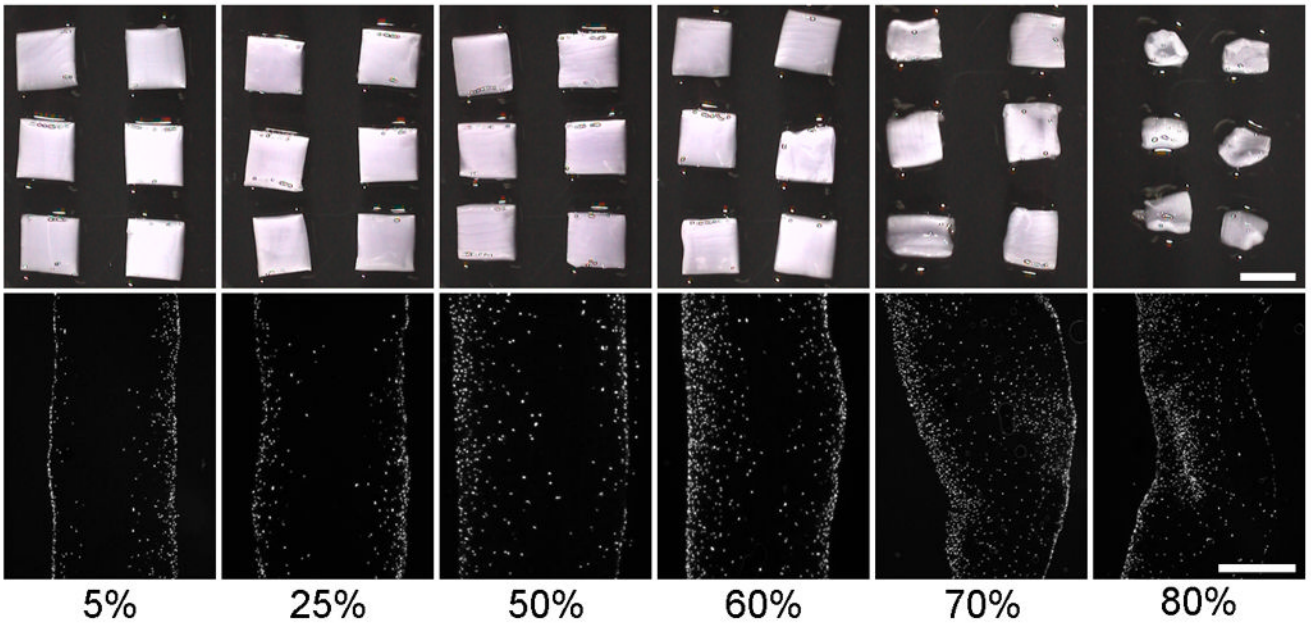

Figure 5. Increasing removal of sacrificial fiber content promotes mesenchymal stem cell (MSC) infiltration into composite fibrous scaffolds

Gross morphology (top row) and DAPI-stained cross-sections (bottom row) of MSC-seeded scaffolds with varying % PEO contents (% mass loss) after three weeks of in vitro culture. Scale bars: 5mm (top), 500μm (bottom).

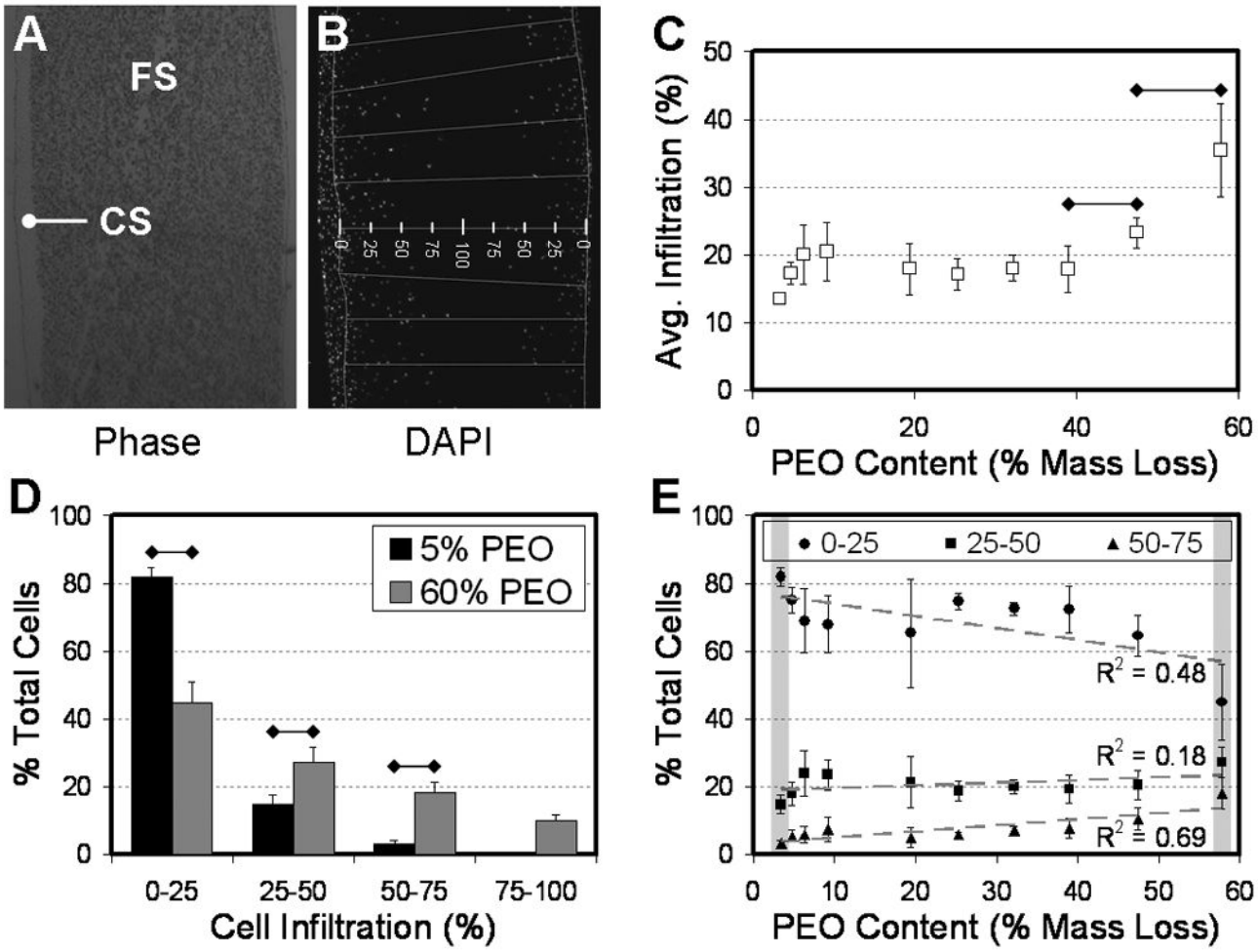

Figure 6. Quantification of MSC infiltration into composite scaffolds as a function of sacrificial fiber content

Corresponding phase (A) and fluorescent (B) images of DAPI-stained construct cross-sections were used to evaluate cellular infiltration into composite scaffolds. (C) The average % infiltration increased in scaffolds above a threshold of ~40% PEO content in the as-spun scaffolds. To quantify cell distribution, infiltration distance was binned with respect to scaffold thickness, as shown in (B). (D) Comparisons of the lowest (~5%) and highest (~60%) PEO content constructs analyzed showed significantly higher fractions of cells within the more central regions of the scaffolds with increased PEO content. (E) The degree of cellular infiltration (as indicated by the % of total cells in each bin) showed a linear correlations with of % PEO content across a range of scaffold compositions. Diamond-ended bars (◆) indicate significance differences observed with $p<0.05$. A total of six samples were analyzed at each level of PEO content.

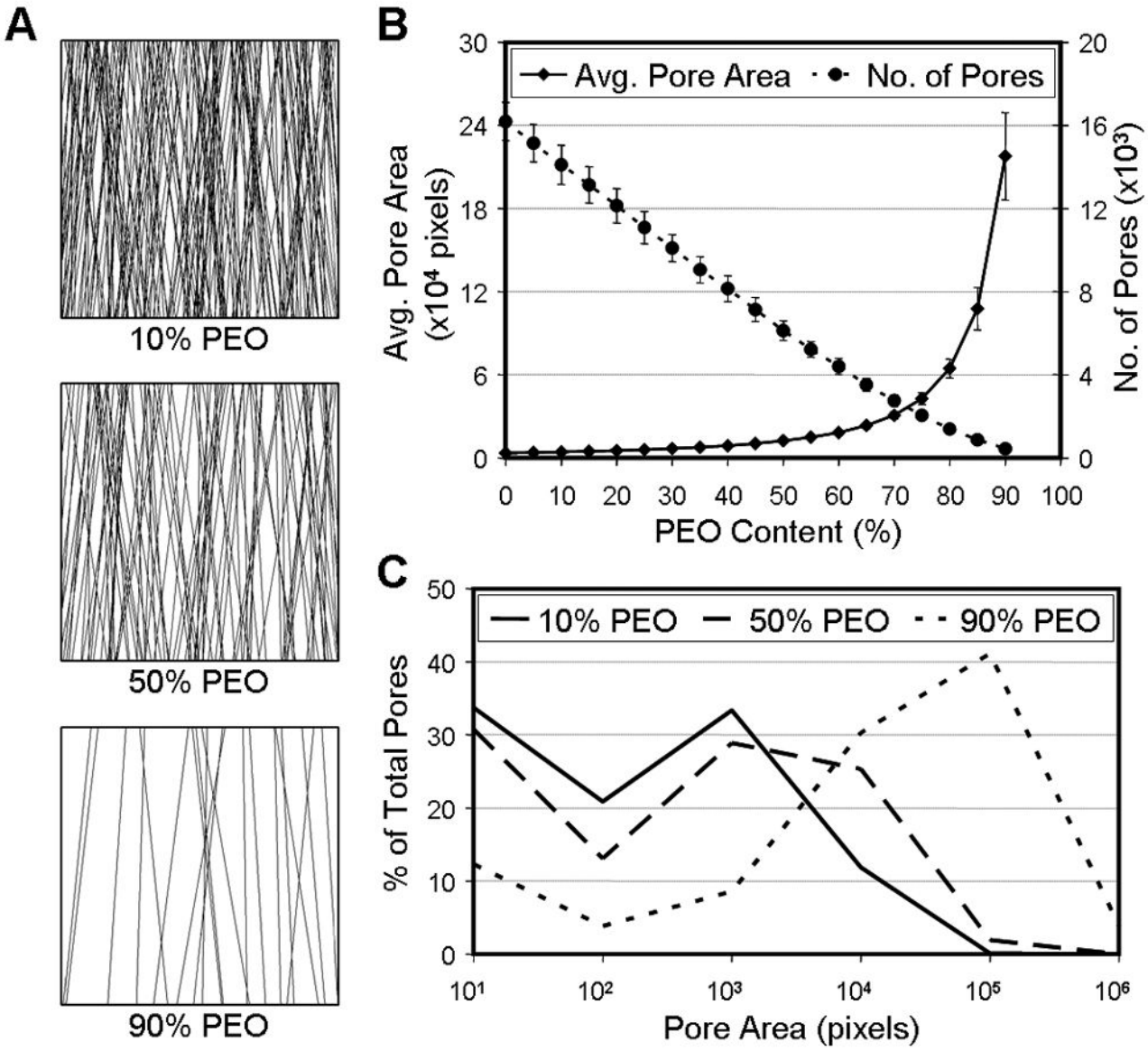

Figure 7. A simple model of composite scaffolds with increasing sacrifical fiber revmoval shows a reduction in pore number, but an increase in average pore size

(A) Example composite scaffold layers representing scaffolds with 10, 50, and 90% sacrificial PEO fibers. (B) Increasing the PEO fiber fraction decreases the total number of pores (●) while increasing the average pore area (◆). (C) Pore area distribution shifts towards higher pore sizes with increasing PEO content. Data were averaged from 20 model iterations, each with a randomly generated fiber population.